Signal complexity of human intracranial EEG tracks successful associative memory formation across individuals

Timothy C. Sheehan[1*], Vishnu Sreekumar [1*], Sara K. Inati [2], and Kareem A. Zaghloul[1 †]

[1] Surgical Neurology Branch, NINDS, National Institutes of Health, Bethesda, MD 20892

[2] Office of the Clinical Director, NINDS, National Institutes of Health, Bethesda, MD 20892

[*]These authors contributed equally to this work.

Draft Date: August 23, 2017
Number of Figures: 5
Number of Tables: 1
Number of Pages: 35

Number of words:
Abstract 148 words
Introduction 619 words
Discussion 1806 words

Acknowledgements: This work was supported by the intramural research program of the National Institute for Neurological Disorders and Stroke. We are indebted to all patients who have selflessly volunteered their time to participate in this study. We thank John Wittig Jr. and Julio Chapeton for helpful comments on the manuscript.

The authors declare no competing financial interests.

[†]**Correspondence should be addressed to:**
Kareem A. Zaghloul
Surgical Neurology Branch, NINDS, National Institutes of Health Building 10, Room 3D20
10 Center Drive Bethesda, MD 20892-1414
Office: (301) 496-2921
Email: kareem.zaghloul@nih.gov

Abstract

Memory performance is highly variable between individuals. Most studies examining human memory, however, have largely focused on the neural correlates of successful memory formation within individuals, rather than the differences between them. As such, what gives rise to this variability is poorly understood. Here, we examined intracranial EEG (iEEG) recordings captured from 43 participants implanted with subdural electrodes for seizure monitoring as they performed a paired-associates verbal memory task. We identified three separate but related signatures of neural activity that tracked differences in successful memory formation across individuals. High performing individuals consistently exhibited less broadband power, flatter power spectral density (PSD) slopes, and greater complexity in their iEEG signals. Furthermore, within individuals across three separate time scales ranging from seconds to days, successful recall was positively associated with these same metrics. Our data therefore suggest that memory ability across individuals can be indexed by increased neural signal complexity.

Significance Statement

We show that participants whose intracranial EEG exhibits less low frequency power, flatter power spectrums, and more sample entropy overall are better able to memorize associations, and that the same metrics track fluctuations in memory performance across time within individuals. These metrics together signify greater neural signal complexity which may index the brain's ability to flexibly engage with information and generate separable memory representations. Critically, the current set of results provide a unique window into the neural markers of individual differences in memory performance which have hitherto been underexplored.

Introduction

Some people consistently have better memory than others. This variability in memory performance between individuals, and even within individuals from moment to moment, is quite familiar in our daily lives. In the study of memory, however, this variability has largely been viewed as a problem that needs to be addressed through proper experimental design. As a result, the neural mechanisms that give rise to such variability have been relatively unexplored. Understanding the source of such variability between individuals can provide valuable insights into how the brain is able to successfully form and retrieve memories.

Studies of memory have typically attempted to eliminate the variability in neural activity and memory performance between individuals by regressing it out. In many paradigms evaluating memory-related changes in oscillatory activity, for example, data within each individual are normalized so as to only examine relative changes in activity when events are either successfully remembered or forgotten, yielding what has been termed the subsequent memory effect (SME). Positive and negative SMEs have been reported in different frequency bands (Hanslmayr and Staudigl, 2014; Hanslmayr et al., 2012), yet how these effects should be properly interpreted has been problematic given conflicting reports of positive low frequency SMEs in some studies (Hanslmayr et al., 2011; Osipova et al., 2006; Sederberg et al., 2003) and negative low frequency SMEs in others (Fell et al., 2011; Guderian et al., 2009; Sederberg et al., 2006). Hence, normalized SMEs studied in isolated frequency bands may not provide a complete description of the neural correlates of memory. Moreover, these approaches have not addressed the larger question of how variability in neural activity may be related to variability in memory performance.

An alternative and complementary approach that has emerged in response to the conflicting SME data is to describe the changes in low and high frequency activity as arising from the same phenomenon, one that produces an overall change in the structure of the entire power spectral density (PSD) (Voytek et al., 2015). Spectral power decreases linearly with frequency on a log-log scale over a broad range of frequencies (Dehghani et al., 2010; He et al., 2010; He, 2014; Miller et al., 2009; Milstein et al., 2009). Importantly, neuronal activation results in a flatter PSD slope (He, 2011), reflecting decreases in lower frequency and increases in higher frequency power (Podvalny et al., 2015). These findings have led to the suggestion that flattening of the PSD slope, and the associated changes in spectral power, may therefore be a signature of increased asynchronous neuronal activity (Burke et al., 2015; Ray and Maunsell, 2011; Voytek and Knight, 2015).

Viewed from an information coding perspective, the PSD slope and oscillatory power of a neural signal, by indicating the extent of synchrony in the underlying neural activity, may be a proxy for neural signal complexity and underlying information content (Hanslmayr et al., 2012). Direct measures of complexity of neural signals such as sample entropy have supported this suggestion by demonstrating that more complex brain dynamics underlie enhanced cognitive performance (McIntosh et al., 2008), likely signifying a greater capacity to encode and process information. Indeed, several groups have advanced the notion that complexity in neural activity is functionally relevant and affords greater flexibility for cognitive processing (Deco et al., 2009,0; Faisal et al., 2008; Garrett et al., 2011,0; Grady and Garrett, 2014; MacDonald et al., 2006; Sleimen-Malkoun et al., 2015; Stein et al., 2005). Therefore, these metrics may together reflect a general capacity for processing information that may be particularly relevant

for memory formation.

In this scenario, then, a possible explanation for the variability in memory performance between individuals is that different brains may exhibit differences in complexity, allowing a greater number of unique cognitive states that are relevant for encoding memories. We investigate this possibility here by examining changes in spectral power, PSD slope, and the sample entropy of neural signals captured from intracranial electrodes as participants perform a paired associates verbal episodic memory task. We were specifically interested in whether these metrics exhibit differences between individuals, and changes within individuals across time, that correlate with memory performance, and find that such measures of complexity and general information processing are indeed behaviorally relevant when forming and retrieving memories.

Materials and Methods

Participants

43 participants [23 male; age range 13-59; 32.1 ± 11.7 (mean ± SD) years old], with drug resistant epilepsy underwent a surgical procedure in which platinum recording contacts were implanted subdurally on the cortical surface as well as deep within the brain parenchyma. For each participant, the clinical team determined the placement of the contacts so as to best localize epileptogenic regions (see Figure 1C for electrode coverage). Preoperative clinical fMRI testing results were available for 37 participants, and 36 of these participants exhibited fMRI activity consistent with left language dominance. The Institutional Review Board (IRB) approved the research protocol, and informed consent was obtained from the participants or their guardians. Data from a subset of participants were initially collected and analyzed for previous publications (Yaffe et al., 2014, 2017; Greenberg et al., 2015; Haque et al., 2015). Computational analyses were performed using custom written MatLab (The MathWorks, Inc., Natick, MA) scripts.

Paired associates task

Each participant performed a paired associates verbal memory task (Figure 1A). In the task, participants were sequentially shown a list of word pairs (encoding period) and then later cued with one word from each pair selected at random (retrieval period), and were instructed to say the associated word into a microphone. Each participant performed one of two versions of the task that had slight differences in the experimental details. As the tasks did not differ in the fundamental objectives and performance was indistinguishable between groups, we combined the data from both sets of tasks for subsequent analyses.

A single experimental session for each participant consisted of 15 or 25 lists, where each list contained either four or six pairs of common nouns shown on the center of a laptop screen, depending on whether the participant completed the first or second version of the task respectively. Although different participants performed the task with different list lengths, the number of pairs in a list was kept constant for each participant. Words were chosen at random and without replacement from a pool of high-frequency nouns and were presented sequentially and appeared in capital letters at the center of the screen. Study word pairs were separated from their corresponding recall cue by a minimum lag of two study or test items. During the study period (encoding), each word pair was preceded by an orientation stimulus (either a '+' or a row of capital X's) that appeared on the screen for 250-300 ms followed by a blank interstimulus interval (ISI) between 500-750 ms. Word pairs were then presented stacked in the center of the screen for 2500 ms followed by a blank ISI of 1500 ms with a jitter of 75 ms in the first version of the task, or for 4000 ms followed by a blank ISI of 1000 ms in the second version. Following the presentation of the list of words pairs in the second version of the task, participants completed an arithmetic distractor task of the form A + B + C = ? for 20 seconds.

In both task versions, during the test period (retrieval), one word was randomly chosen from each of the presented pairs and presented in random order, and the participant was asked to recall the other word from the pair by vocalizing

a response. Each cue word was preceded by an orientation stimulus (a row of question marks) that appeared on the screen for 250-300 ms followed by a blank ISI of 500-750 ms. Cue words were then presented on the screen for 3000 ms followed by a blank ISI of 4500 ms in the first version of the task, or for 4000 ms followed by a blank ISI of 1000 ms in the second version. Participants could vocalize their response any time during the recall period after cue presentation. We manually designated each recorded response as correct, intrusion, or pass. A response was designated as pass when no vocalization was made or when the participant vocalized the word 'pass'. We defined all intrusion and pass trials as incorrect trials. A single experimental session therefore contained 60, 100, or 150 total word pairs, or trials, depending on the task version. We included only participants who engaged in at least two separate sessions of the paired associates task such that each participant completed between 2-5 sessions taking 31.1 $\pm$ 1.7 (mean $\pm$ SEM) minutes each with a median of 24.8 hours in between sessions.

Intracranial EEG (iEEG) recordings

Intracranial EEG (iEEG) signals were referenced to a common electrode and were resampled at 1000 Hz. We applied a fourth order 2 Hz stopband butterworth notch filter at 60 Hz to eliminate electrical line noise. The testing laptop sent synchronization pulses via an optical isolator into a pair of open lines on the clinical recording system to synchronize the iEEG recordings with behavioral events.

We collected electrophysiological data from a total of 4623 subdural and depth recording contacts (PMT Corporation, Chanhassen, MN; AdTech, Racine, WI). Subdural contacts were arranged in both grid and strip configurations with an inter-contact spacing of 5 or 10 mm. Contact localization was accomplished by co-registering the post-op CTs with the post-op MRIs using both FSL Brain Extraction Tool (BET) and FLIRT software packages and mapped to both MNI and Talairach space using an indirect stereotactic technique and OsiriX Imaging Software DICOM viewer package. The resulting contact locations were subsequently projected to the cortical surface of a population average brain. Pre-op MRI's were used when post-op MRI images were were not available.

We analyzed iEEG data using bipolar referencing in order to reduce volume conduction and confounding interactions between adjacent electrodes (Nunez and Srinivasan, 2006). We defined the bipolar montage in our dataset based on the geometry of iEEG electrode arrangements. For every grid, strip, and depth probe, we isolated all pairs of contacts that were positioned immediately adjacent to one another; bipolar signals were then found by differencing the signals between each pair of immediately adjacent contacts. The resulting bipolar signals were treated as new virtual electrodes (referred to as electrodes throughout the text), originating from the mid-point between each contact pair. All subsequent analyses were performed using these derived bipolar signals. In total, our dataset consisted of 3904 bipolar referenced electrodes.

To minimize the effect of epileptic activity and physiology on our signals, we performed an electrode cleaning procedure to eliminate electrodes that demonstrated ictal or interictal activity at any time during clinical monitoring as reviewed by an epileptologist. We had access to this data for 27 individuals and it included 419 electrodes. After excluding these pairs from further analysis, we were left with 3485 bipolar pairs upon which we performed an additional variance based cleaning procedure. For each subject we looked at the spread of variance across electrodes

and iteratively removed electrodes that exceeded 1.3 standard deviations from the the average of the remaining electrodes until no additional electrodes exceeded this threshold. This procedure eliminated 758 electrodes leaving 2727 bipolar pairs for our study.

Data analyses and spectral power

We computed the spectral power for each bipolar electrode at every time point during the experimental session by convolving the raw iEEG signal with complex valued Morlet wavelets (wavelet number 6) to obtain the magnitude of the signal at each of 30 logarithmically spaced frequencies ranging from 3 to 180 Hz. We squared and log-transformed the magnitude of the continuous-time wavelet transform to generate a continuous measure of instantaneous power. During every trial, we convolved each wavelet with two separate time windows - a baseline period extending from 600 to 100 ms before word pair presentation, and an encoding period from 300 ms after word pair presentation until 300 ms before the offset of the word pair from the display screen (Figure 1A). In addition, we computed power for ten 2000 ms windows from the beginning of the clinical recording segment before task specific activity began for each session and averaged those to get an extra-task window. We included an additional 1000 ms buffer on either side of each time window to minimize any edge effects and which was not subsequently analyzed.

To examine the relation between overall raw power and performance across participants, we used the above measures of raw spectral power. To examine how changes in power on individual trials affected performance, we z-scored each sessions power values independently to remove the effects of across participant and session level variations.

Calculating spectral slope

To understand how spectral power changes as a function of frequency, we calculated spectral slope. For each participant, we computed an average power spectral density (PSD) across all trials and electrodes and computed slope in log-log space across the broadband range of 10-100 Hz (Podvalny et al. (2015)). To identify the general $\frac{1}{f^{\alpha}}$ slope of the spectrum and avoid contamination of narrowband oscillations, we used a robust fitting algorithm with bisquare weighting (MATLAB *robustfit.m* function). Additionally, we computed slope over a range of frequency values and spectral widths as described in the Results. We defined spectral width using units of octaves such that the spectral width of a given slope was equal to the log_2 of the ratio of the highest frequency to the lowest frequency.

Calculating sample entropy

We used a metric of sample entropy to measure the complexity of the iEEG signal. Sample entropy, by construction, is a measure of predictability. Specifically the sample entropy (SampEn) of a time series is the negative natural logarithm of the conditional probability that any two sub-sequences of length m within the series, that are similar within a tolerance r, remain similar at length m+1 (Richman and Moorman, 2000). Two patterns that are close together in m-dimensional space and that remain close together in m+1-dimensional space indicate fewer irregularities or less complexity in the signal. Similarity is measured using the Chebychev distance between the two sub-sequences.

A smaller value of SampEn denotes greater repetitiveness and less complexity in a given signal.

For an embedding dimension m, a tolerance r, and a time-step τ, the formal equations for the calculation of sample entropy for a given time series y(t) are as follows (Sokunbi et al., 2013; Vakorin and McIntosh, 2012):

$$SampEn(m, r, N) = -ln\frac{U^{m+1}(r)}{U^m(r)} \tag{1}$$

$$U^m(r) = [N - m\tau]^{-1} \sum_{i=1}^{N-m\tau} \frac{B_i}{N - (m+1)\tau} \tag{2}$$

$$B_i = \sum_{j \neq i}^{N-m} \mathcal{H}[r - ||x_m(i) - x_m(j)||] \tag{3}$$

where $x_m(i)$ refers to the i^{th} possible template vector of length m, such that $x_3(2) = (y_2, y_3, y_4)$. $||\cdot||$ refers to the maximum norm and $\mathcal{H}$ is the Heaviside step function.

An embedding dimension m of 2, a tolerance r of $0.2 * std(x(t))$, and a constant time-step τ of 1 ms were used in all analyses. Of note, the number of 3 element matching template sequences is necessarily less than or equal to the number of 2 element matching template sequences, implying that the ratio $\frac{U^{m+1}(r)}{U^m(r)}$ in Equation 1 is bounded between 0 and 1. Therefore, the range of SampEn is $[0, \infty]$. For computational considerations, we down-sampled all iEEG signals to 250 Hz for this analysis. We excluded the few trials with zero matching samples of length 3 to avoid infinite values.

Commonality Analysis

In order to understand whether the metrics of power, spectral slope, and sample entropy uniquely account for variance in memory performance across participants or if they are redundant, we performed a commonality analysis (Nimon et al., 2008) which partitions variance (R^2) into parts that are unique to each predictor variable and those that are shared between all possible combinations of the predictors. The unique contribution of a predictor is calculated as the proportion of variance attributed to it when it is entered last in a regression analysis. For example, in a hypothetical case where dependent variable y is explained by two predictors i and j, the total variance explained by both variables is R^2 and the unique contributions from i and j respectively are

$$U_{(i)} = R^2_{y.ij} - R^2_{y.j} \tag{4}$$

$$and$$

$$U_{(j)} = R^2_{y.ij} - R^2_{y.i}. \tag{5}$$

$$\tag{6}$$

The common contribution is

$$C_{(i,j)} = R^2_{y.i} + R^2_{y.j} - R^2_{y.ij}. \tag{7}$$

Commonality analysis decomposes explained variance into $2^k - 1$ independent effects for k predictor variables. Therefore the number of effects increases exponentially with the number of predictors. We used the R package *yhat* (Nimon et al., 2013) to perform commonality analysis.

Anatomic visualization

To visualize how the relation between spectral power and task performance is spatially distributed, we created 1441 regions of interest (ROI) evenly spaced across a 1 cm x 1 cm grid covering the pial surface of a population average brain. In each participant, we identified all electrodes located within 12.5 mm of each ROI. We designated the raw power for each ROI in each participant as the average raw power across all electrodes assigned to that ROI. For each ROI that included electrodes from at least six participants, we determined the Spearman's correlation between raw power and task performance across the participants with electrodes contributing to that ROI. We therefore generated a value for the correlation between raw power and task performance for each ROI. Any ROI that contained electrodes from fewer than six participants was excluded from statistical analyses.

We generated cortical topographic plots of the anatomic distribution of these correlations by assigning each vertex in the 3D rendered image of the standard brain a weighted average of the mean value of each ROI that includes that vertex. Weighted values for each vertex were assigned by convolving a three dimensional Gaussian kernel (radius = 12.5 mm; σ =4.17 mm) with center weight 1 with the values of surrounding ROIs. We projected these vertex values onto the standard brain. Intensity varied as a function of the statistic metric in question, either Fisher-transformed correlation or t-score, in each ROI and with the standard deviation of the Gaussian kernel, which was used purely as a visualization technique.

Statistical analysis

All statistical tests were assessed for significance using two-tailed distributions. As most of our distributions, including accuracy and raw power were not normally distributed, we utilized Spearman's rank correlation when evaluating the monotonic relationship between two variables. Spearman's correlation utilizes only the order of data points and is thus not biased by outliers as with Pearson's correlation. We made an exception, however, when examining the relation between sessions within individual participants. Because we analyzed session counts as low as three, Spearman's correlation is prone to produce extreme values of ± 1 which cannot be analyzed with cohort level statistics, necessitating the use of Pearson's correlation in this instance.

To compare correlations across participants, we used a Fisher z-transformation on the correlation coefficients calculated for each participant. The transformation stabilizes the variance of these correlations, reduces bias towards lower correlations, and results in a normalized distribution of coefficients. For each correlation, we therefore calculated

the Fisher z-transform: $z = \frac{1}{2} ln\left(\frac{1+r}{1-r}\right)$ where r is the correlation coefficient. We utilized the mathematically equivalent formula, $z = arctanh(r)$ in our calculations.

To determine whether any anatomic region exhibited a significant correlation across participants, we used a nonparametric spatial clustering procedure (Maris and Oostenveld, 2007). This procedure identifies contiguous ROIs where the distribution of correlation coefficients across participants significantly deviates from chance correlation while controlling for the family-wise error rate. Briefly, for each ROI, we calculated the true Fisher-transformed correlation coefficient between memory performance and raw spectral power across participants. We then generated 1000 permuted values for each ROI. In each permutation, we randomly assigned each participant a level of task performance drawn from the original distribution of task performance across participants without replacement. In this manner, each permutation involves a random pairing between task performance and raw spectral power. We then determined a z-score for each true value and each permuted value in each ROI by comparing that value to the distribution of permuted values. For the true data and for each permutation, we identified contiguous spatial clusters of ROIs, exhibiting z-scores with a magnitude greater than 1.96 (corresponding to a two-tailed p-value less than 0.05). For each cluster, we computed the cluster statistic as the sum of all z-scores in that cluster. In this manner, large magnitude cluster statistics can arise from large deviations in the distributions of correlation coefficients across participants extending over a small spatial region, or moderate deviations that extend over larger regions. We then calculated the exact two-tailed p-value for each cluster observed in the true dataset by comparing its cluster statistic to the distribution of largest cluster statistics drawn from each permutation. Clusters were determined to be significant and corrected for multiple comparisons if their p value calculated in this manner was less than 0.05.

To assess whether the relation between sample entropy and performance at different time scales was significantly from zero when summarizing across participants, we used a similar permutation procedure. In this case, for every ROI, we used a two-tailed t-test to compare the distribution of values to zero. This generates a t-statistic for the true data. Then, during every permutation, we randomly inverted the sign of the metric and produced a permuted distribution of t-statistics. We compared the true t-statistic to the permuted distribution to generate a p-value and z-score for every ROI. As above, we used a clustering procedure to identify contiguous ROIs with $p < 0.05$, assigned each contiguous cluster a cluster statistic based on the sum of the corresponding t-statistics, and then calculated the exact two-tailed p-value for each cluster observed in the true dataset by comparing its cluster statistic to the distribution of largest cluster statistics drawn from each permutation.

Results

43 participants with drug resistant epilepsy who underwent surgery for placement of intracranial electrodes for seizure monitoring participated in a verbal paired associates task (Figure 1A). Participants studied 294.2 ± 20.0 (mean ± SEM) word pairs, split across multiple experimental sessions, and successfully recalled 40.1 ± 3.2% (mean ± SEM) words with a mean response time of 1837 ± 65 ms. Response accuracy across participants exhibited a bimodal distribution (Figure 1B). On 14.9 ± 1.7% of trials, participants responded with an incorrect word (intrusions) with a mean response time of 2687 ± 83 ms. For the remaining 44.9 ± 2.6% of trials, participants either made no response to the cue word, or vocalized the word 'pass' with a mean response time of 3494 ± 176 ms. We designated all trials in which a participant successfully vocalized the correct word as correct, and all other trials as incorrect. Recordings were included from all electrode contacts (number of participants with contacts in each cortical location shown in Figure 1C).

We measured full scale IQ (FSIQ) in 36 participants before electrode implantation as part of the routine clinical pre-operative evaluation. Participants had an average pre-operative FSIQ of 98.5 ± 2.8 (mean ± SEM). Across all sessions for each participant, we found that preoperative FSIQ significantly correlated with accuracy during the task ($r_s = 0.55$, $p = .0005$, $N = 36$; Figure 1D), suggesting that task performance is related to normal psychometric measurements.

– INSERT FIGURE 1 –

Raw power is negatively correlated with performance

Raw intracranial EEG (iEEG) power can reflect the extent of overall neural activity in each participant's brain and has occasionally been shown to relate to a participant's abilities (Hanslmayr et al., 2007). We were therefore interested in examining whether the raw overall power in each participant as captured by iEEG was related to their task performance. As typical spectral analysis involves examining changes in z-scored power relative to an individual's baseline activity, this relation between raw power and task performance would be unexplored in most planned analyses.

In each participant, we extracted the raw spectral power contained in the signal during a baseline time window before word pair presentation and during the encoding period. To generate an overall level of broadband power for each participant, we averaged the extracted spectral power over all frequencies between 3 and 180 Hz (broadband power), over all trials, and over all electrodes for each time window in each participant. We found that the average raw broadband power during the encoding period demonstrated a significant negative correlation with accuracy during the task ($r_s = -0.42$, $p = .0051$, $N = 43$; Figure 2A). As with task performance, broadband power was also negatively correlated with with FSIQ across participants ($r_s = -0.47$, $p = .0043$, $N = 36$).

We found that this relation between raw overall broadband power and task performance was robust and independent of the specific task periods. For example, raw broadband power during the baseline period before word presentation was also inversely correlated with task accuracy ($r_s = -0.42$, $p = .0052$, N=43). Moreover, we also

found a significant relation between raw broadband power and task accuracy when we examined power separately during only correct or only incorrect trials ($r_s = -0.42$, $p = .0055$ and $r_s = -0.42$, $p = .0051$, respectively), suggesting that this effect reflects each participant's overall baseline neural activity rather than simply the proportion of trials that featured successful encoding in each participant. Finally, to determine if this relation reflects each participants underlying physiology or is dependent on a task evoked state, we also examined this relation during an epoch recorded prior to the beginning of the task when the participant was awake, at rest, and under no instruction. We found the negative correlation between overall broadband power and task performance was also preserved during this extra-task period, suggesting that this effect is not task dependent but is related to baseline cognitive behavior ($r_s = -0.40$, $p = .0090$). This finding departs from most memory studies in that we claim that our result does not depend on the fact that the subject is undertaking a memory task at the time, allowing us to generalize our electrophysiological correlates to normal daily activities.

We next examined whether the inverse correlation between raw power and task performance was specific to individual frequency bands by separately computing correlations between narrow band frequencies and task performance (Figure 2B). We found power at every frequency band between 3 and 180 Hz was negatively correlated with performance. All frequencies below 9 Hz had a significant negative correlation between overall raw power and accuracy when corrected for multiple comparisons across frequencies (Figure 2B, $p < .05$, Bonferroni corrected for 30 frequency bands). This suggests that this effect is spectrally broad but driven by low frequency activity. We therefore restricted subsequent power analyses to power averaged across the theta band (3-7 Hz; Figure 2B, dashed box).

We were also interested in whether the relation between raw power and task accuracy varied across brain regions (regions of interest, ROIs; see Materials and Methods). For every ROI, we determined the correlation between both average raw broadband and theta power in all electrodes within that ROI and task performance across participants. The inverse correlation that we found between cortically distributed raw power and task performance localized to regions of the temporal and parietal lobes in both hemispheres (Figure 2C,D, *top*). Using a non-parametric clustering algorithm, we found that spatially contiguous regions exhibited a significant correlation across participants within the left temporal lobe for both broadband and theta band power ($p < .05$, permutation procedure; see Materials and Methods; Figure 2C,D, *bottom*). In addition theta band power showed a significant cluster in the right anterior temporal lobe suggesting that this effect is not confined to one hemisphere. These data suggest that individuals with less broadband and low frequency power in their temporal lobes in general have greater ability to encode associative memories.

– INSERT FIGURE 2 –

Assessing cortical activation through PSD slope

The power spectral density (PSD) of iEEG signals falls off with frequency following a power law distribution. The slope of the PSD in log-log space has been shown to flatten in response to task activation (Podvalny et al., 2015), and the extent to which the slope flattens has been related to cognitive effort (Churchill et al., 2016). As such, we

examined the overall raw PSD in each participant to determine whether the observed changes in broadband power with task performance may be related to changes in the slope of the PSD.

We first divided the participants into three terciles based on task performance (low, medium, or high accuracy) to visualize the average raw PSD in each cohort (Figure 3A). Below 30 Hz, the average PSDs of the three populations easily separate, with the lowest performing participants exhibiting the largest low frequency raw power. As suggested by our analysis examining the correlation between raw power and task performance, dividing participants into these terciles yielded a significant effect of performance tercile on low frequency power (ANOVA using average raw power < 30 Hz; $F(2, 40) = 5.07$, $p = .011$). At higher frequencies (> 30 Hz), however, the distinction between participant groups was negligible ($F(2, 40) = 1.21$, $p = .308$).

We next calculated the spectral slope of the average raw PSD between 10-100 Hz for each participant (Figure 3B, *insert*). We chose this frequency range to avoid the low frequency knee and the effects of action potential contamination at higher frequencies (Podvalny et al., 2015). Across participants, PSD slope [range -3.33 to -2.06; -2.68 $\pm$ .05 (mean $\pm$ SEM) Figure 3B)] are in the range of those reported by those using similar metrics (Podvalny et al., 2015). Across participants, we found that PSD slope was positively correlated with task performance, such that participants with flatter slopes performed better ($r_s = 0.49$, $p = .0011$, $N = 43$; Figure 3C). We examined the anatomic regions that demonstrated a significant relation between PSD slope and task performance ($p < .05$, permutation procedure) and localized them to the left frontal and left temporal lobes (Figure 3D).

As with raw broadband and theta power, this relation between PSD slope and task performance was robust and independent of when during the task the calculation of PSD was made. We found participants with greater task performance had flatter slopes when examining recordings from the baseline period ($r_s = 0.47$, $p = .0016$), during correct trials only ($r_s = 0.47$, $p = .0016$), or during incorrect trials only ($r_s = 0.48$, $p = .0011$). We found that like broadband power, the significant relationship between slope and accuracy was preserved when examining extra-task epochs during which participants were awake and at rest ($r_s = 0.44$, $p = .0035$), indicating that as with raw power, this relation is not task evoked. Of note, we found no flattening of slope with age as has been reported elsewhere ($r_s = -0.19$, $p = .24$) (Voytek et al., 2015).

Although several studies have identified measures of broadband power or spectral slope as a proxy for spike rate (Manning et al., 2009), cortical activation (Podvalny et al., 2015), or the balance between cortical excitation and inhibition (Gao et al., 2017), there still remains no consensus regarding the frequency range over which one should calculate the PSD slope in order to identify the non-oscillatory components of spectral power. In our initial analysis, we used a range of 10-100 Hz. However, other groups have used different frequency ranges and it is possible that our findings are sensitive to this parameter.

To ensure that the observed relation between PSD slope and task performance was not specific to the range of frequencies we used to calculate PSD slope, we iterated through a library of different frequency windows, each comprised of a center frequency and a spectral width, to compute PSD slopes. We examined PSD slope using every possible frequency window between 3 and 180 Hz. We found that the slope was largely unaffected by spectral width, and that although the slope increased as a function of center frequency, beyond a center frequency of 20 Hz, average

slope stabilized to an overall mean across participants of approximately 2.7 (Figure 3E). Above 18 Hz, the PSD slopes ranged between -2 and -3 , while at lower center frequencies we observed PSD slopes as flat as -1. We examined how varying our measure of PSD slope affected the relation between PSD slope and task performance. We correlated each PSD slope calculated with different center frequencies and spectral widths with task performance and confirmed that PSD slopes were positively correlated with task accuracy for most center frequencies regardless of spectral width (Figure 3F). This suggests that when examining the role of spectral slope, most ranges centered above 20 Hz should give congruent results.

– INSERT FIGURE 3 –

Assessing information content through sample entropy

The relation between spectral slope and accuracy may be partially explained by the complexity of the underlying iEEG signal which may in turn suggest a higher capacity for processing information. However, while spectral slope is related to signal complexity (Keshner, 1982), it is not a direct measure. We therefore calculated sample entropy to quantify signal complexity of the iEEG trace, a measure that has previously been successfully used for discerning differences between EEG signals (Figure 4A; see Materials and Methods) (Catarino et al., 2011; Mizuno et al., 2010; Vaz et al., 2017). Sample entropy measures the predictability of a signal, is robust to low level noise and artifacts, and has been found to be more robust for shorter data lengths than other measures of entropy such as approximate entropy (Sokunbi, 2014; Yentes et al., 2013). Indeed, the complexity of two example iEEG signals is visible in the raw recording and reflected in the measured sample entropy (Figure 4B).

Based on the observed changes in raw power and spectral slope, and the theoretical suggestion that increased information content involves signal desynchronization (Hanslmayr et al., 2012), we hypothesized that participants with greater complexity in their iEEG signal, and therefore higher sample entropy, would exhibit better task performance. We calculated the average sample entropy during the encoding period across all trials and all electrodes and found that participants with greater sample entropy performed significantly better on the task (Figure 4C, $r_s = 0.57$, $p = .0001$, $N = 43$), suggesting that the observed relation between task performance and PSD slope is related to the complexity of the underlying neural signal. The relation between sample entropy and accuracy was distributed across the cortex but was particularly localized to the left temporal lobe (Figure 4D).

As with power and spectral slope, we found that this relation was preserved when looking at correct trials ($r_s = 0.52$, $p = .0004$), incorrect trials ($r_s = 0.58$, $p = .000010$), the baseline period ($r_s = 0.56$, $p = .0001$), or an extra-task epoch ($r_s = 0.41$, $p = .0070$). Moreover, participants with flatter PSD slopes and less theta power had greater sample entropy ($r_s = 0.66$, $p = 3.6 \times 10^{-6}$ and $r_s = -0.45$, $p = .0030$, respectively) demonstrating that spectral slope and low frequency power are strong indicators of signal complexity.

– INSERT FIGURE 4 –

Signal complexity across time scales

Our data demonstrate that related measures of signal complexity — low frequency power, spectral slope, and sample entropy — show strong relations with overall performance during an associative memory task across participants. However, most studies of human memory have focused on subsequent memory effects in which differences between correct and incorrect trials are assessed within individuals. We were therefore interested in whether the observed changes in neural signal complexity across participants would also be observed across different time scales within participants. We specifically investigated changes in sample entropy during individual sessions and trials to index changes in brain state complexity at the time scales of hours and seconds, respectively.

We first examined the relation between sample entropy and performance during individual sessions for each electrode in each participant who completed at least three sessions. In individual participants, we found that sample entropy correlated with performance on a session by session basis (Figure 5A). Across all participants, we found that this relation was consistent and significantly greater than zero (t-test of Fisher transformed correlation coefficients, $t(21) = 3.55$, $p = .0019$, N=22; Figure 5B). We found that the relation between session level sample entropy and task performance localized to the left anterior temporal lobe (Figure 5C).

To ensure this effect was not driven by item level differences between sessions in entropy, we initially restricted this analysis to only correct trials. However, when we examined all trials together, or when we examined only incorrect trials, we found similar effects suggesting that the observed session level relations are independent of item level effects ($t(21) = 2.71$, $p = .0130$ and $t(21) = 2.125$, $p = .0456$, respectively). Moreover, the rest epochs prior to the task in each session also exhibited a significant positive relation between sample entropy and performance ($t(21) = 2.15$, $p = .0431$).

Next, as is routine in most memory studies, we examined differences between correct and incorrect trials to understand the relation between sample entropy and memory encoding at the time scale of seconds. We first z-scored sample entropy within each session to eliminate any session level variance, and found that participants exhibited significantly higher sample entropy for correct compared to incorrect trials (Figure 5D,E, $t(43) = 3.252$, $p = .0023$). The item level changes in sample entropy localized to the left inferior prefrontal cortex and left posterior temporal lobe (5E). Both the session level and item level effects are calculated such that they are completely independent from one another and the previously explored participant level effects.

From these tests alone, it is unclear over what time scale the changes in sample entropy are occurring. These changes may be related to word pair adaptation, or they may reflect a more slowly fluctuating dynamic. To explore this, we made three additional comparisons. We compared the sample entropy during the baseline period between correct and incorrect trials, we compared the sample entropy during correct trials between the encoding and baseline periods, and we compared the sample entropy during incorrect trials between the encoding and baseline periods. Interestingly, while we found no difference in sample entropy during the baseline periods between correct and incorrect trials ($t(42) = -0.945$, $p = .3501$), we did find that sample entropy significantly increased from baseline during correct trials, and significantly decreased from baseline on incorrect trials ($t(42) = 2.89$, $p = .0060$; $t(42) = -2.68$, $p = .0105$). These data suggest that relatively fast changes in the sample entropy, and therefore complexity, of the

signal contribute to subsequent remembering and subsequent forgetting along with changes over much longer longer time scales.

– INSERT FIGURE 5 –

Are theta power, spectral slope, and sample entropy redundant?

We performed a commonality analysis (Nimon et al., 2008) to determine the proportions of variance in memory performance across participants that are uniquely attributed to the metrics of theta-band power, spectral slope, and sample entropy as well as those that are common between all possible combinations of these metrics, given that the three metrics are correlated with each other. Spectral slope and sample entropy are highly correlated ($r_s(41) = 0.66, p = 1.92 \times 10^{-6}$) as they both index signal predictability. Both spectral slope and sample entropy are negatively and moderately correlated with theta power ($r_s(41)_{Pow,Slope} = -0.42, p = 0.006$; $r_s(41)_{Pow,SampEn} = -0.45, (p = 0.003)$). The commonality analysis (Table 1) showed that spectral power in the theta band uniquely accounted for 37.60% of the total variance explained by the predictors, followed by spectral slope (10.66%), and a much smaller unique contribution from sample entropy (1.25%). Spectral slope and sample entropy together account for 8.77% of the total variance explained. The total variance accounted for by power, PSD slope, and sample entropy though both unique and shared contributions are 0.3082, 0.2144, and 0.1620 respectively. Therefore, the commonality analysis suggests that theta-band spectral power uniquely contributes to a sizeable proportion of the variance explained (by a regression involving all three metrics) in memory performance across participants, whereas spectral slope and sample entropy provide redundant information (as suggested by the high correlation between them) and contribute to the total variance in combination with each other as well as with theta power. Taken together, this analysis suggests that while the three metrics capture properties of neural activity that are relevant for memory performance, theta power may capture somewhat distinct features than those that are captured together by spectral slope and sample entropy.

– INSERT TABLE 1 –

Discussion

Our analyses demonstrate that variability in memory performance between individuals can be partially explained by low frequency power and the slope of the PSD, with each measure providing unique contributions to the total variance explained. We directly link these metrics to sample entropy, a measure of the complexity of the neural signal (Hanslmayr et al., 2012; McIntosh et al., 2008; Sokunbi, 2014). Individuals with brains that exhibit greater complexity in their overall neural activity are able to perform better on this memory task. Moreover, within individuals, the extent to which performance changes from moment to moment is related to the entropy of their neural signals at that time. Hence, our data suggest that the complexity of brain activity may reflect an individual's ability to occupy variable cognitive states and the extent to which information can be coded in their brain signals, which have a direct bearing on memory performance.

The suggestion that cognitive flexibility may improve task performance appears intuitive. Indeed, the ability to explore the brain's dynamic repertoire during rest is thought to be a marker of healthy brain function and may underlie introspection and rehearsal (Ghosh et al., 2008). Therefore, it seems likely that a high performing brain is one that engages with the world by assuming a variety of functional configurations. Whether such variability and flexibility may be relevant for associative memory performance has, until now, not been directly established. We establish this link here by demonstrating that memory performance is significantly correlated with signal complexity both across and within individuals. Cognitive flexibility lends neural systems the ability to explore their state space (Deco and Jirsa, 2012) which may lead to separable memory representations that are less susceptible to interference. Consistent with this idea, Heisz et al. (2012) showed that multiscale entropy (MSE) of brain signals (scalp EEG) correlated with participants' ratings of famous face familiarity and that MSE increased with learning over multiple exposures to previously unfamiliar faces. Hence, the observed correlation between entropy and associative memory performance here suggests that neural signal complexity reflects the capacity to successfully encode associative memories by flexibly engaging with the presented material.

The paired associates memory task used here requires participants to form associations between unrelated words that constitute individual episodes or experiences that are subsequently recalled. Encoding these associations draws upon the meanings of the words in order to form a conceptual and semantic link between them (Jang et al., 2017; Kahana et al., 2008; Madan et al., 2010). Therefore, forming these associations should engage cortical regions such as the anterior temporal lobe that are involved in semantic processing (Binder et al., 2009; Ralph et al., 2017). In our data, we observe strong correlations between memory performance and low frequency power, PSD slope, and entropy in these same left temporal lobe regions. The relationship between cognitive flexibility, as assessed by these metrics in the temporal lobe, and verbal associative memory performance across individuals may therefore emerge because of the involvement of the temporal lobe in helping encode verbal associations.

Our approach here differs from earlier studies of human memory encoding and retrieval by specifically asking whether there are systematic differences in neural activity across participants that may predict individual memory performance. Most previous studies of human episodic memory have focused on relative changes in neural oscillatory activity between correctly and incorrectly encoded events (Burke et al., 2014; Greenberg et al., 2015; Long et al.,

2014; Sederberg et al., 2003, 2007). While these studies have significantly advanced our understanding of the neural correlates of human memory, an unresolved question has been why different studies have demonstrated conflicting results, particularly with respect to low frequency oscillatory power (Hanslmayr and Staudigl, 2014). In our data, we tracked memory performance using low frequency power that was not normalized relative to any baseline and found that it was inversely correlated with overall memory performance. Moreover, within each individual, fluctuations in neural activity were predictive of how well they performed at any given moment. Our data therefore may provide some insight into the conflicting data observed in previous studies. These conflicts have been previously attributed to differences in task design and electrode coverage. However, because of the variability in baseline power between individuals, these conflicts may also be affected by where each cohort of participants sits in this range of baseline power and how that may impact the changes in power observed over shorter time scales.

As examining the structure of the full PSD across all frequencies can often yield a more complete picture of neural activity (Podvalny et al., 2015), our analyses of PSD slope changes complement the observed changes in low frequency power. The PSD usually exhibits a power law distribution, with an exponent α of the $\frac{1}{f^{\alpha}}$ distribution ranging between -2 and -4 (Freeman and Zhai, 2009). Consistent with previous studies (He et al., 2010), we found that the slope of the PSD became flatter when successfully encoding individual memories. Notably, this relation between PSD slope and memory extended to the level of individual participants. Those participants with flatter PSD slopes in their overall brain activity were able to perform the task more successfully.

The slope of the PSD has been hypothesized to reflect the balance between excitation and inhibition, and computational modeling of neural activity has demonstrated that reducing E:I ratio results in a steeper PSD slope (Gao et al., 2017). Both *in vitro* and *in vivo* cortical networks show maximal dynamic range under balanced E:I conditions (Shew et al., 2009,0). An increased dynamical range of neuronal responses may improve adaptability and efficiency of neural systems in service of memory. Another possibility is that a shallower PSD slope may emerge due to the infusion of noise into the neural signal via asynchronous firing activity (Podvalny et al., 2015; Pozzorini et al., 2013; Usher et al., 1995; Voytek et al., 2015; Voytek and Knight, 2015). Whether such noise is beneficial is unclear, as the effect of noise on information coding depends on whether or not noise is correlated between neurons (Averbeck et al., 2006). Nevertheless, our finding that flatter PSD slopes and increased sample entropy relate to better memory performance suggests that in our data, more complex brain signals reflect more informationally rich signals as posited by others (Hanslmayr et al., 2012, 2016; Mitchell et al., 2009; Schneidman et al., 2011).

Ultimately, the slope of the PSD and the low frequency power contributing to that slope should be related to the underlying complexity of the neural signal, which can be directly assessed using measures of entropy as we do here. Although greater signal complexity does not always reflect greater information content, sample entropy of the EEG signal increases from childhood to adulthood (McIntosh et al., 2008), and higher entropy is also associated with greater task efficiency and greater network efficiency (Misić et al., 2010, 2011). Entropy of resting state brain signals can distinguish children at high risk for autism spectrum disorder from normal developing children (Bosl et al., 2011), and healthy from epileptogenic neural tissues (Protzner et al., 2010). Here, we directly show that the complexity of the neural signal captured using iEEG tracks associative memory performance across individuals,

providing further support to the proposition that brain signal variability is functionally relevant. Moreover, we show that within individuals, variability in neural signal complexity across time scales also tracks memory performance for the individual participant. The variability that we experience in our daily lives with memory performance is likely therefore influenced by these changing levels of neural signal complexity.

Of note, participants in our study were also neurosurgical patients with drug resistant epilepsy. In the majority of cases, their seizure activity localized to the temporal lobes, raising the possibility that the observed effects in this brain region may also be related to the underlying pathology of the disorder itself. Greater disruptions of normal temporal lobe function could result in less signal complexity in this brain region, which could then lead to worse memory performance on this paired associates task. We took several precautions to mitigate the effects of epileptic activity on our study including removing electrodes identified as ictal or interictal and removing electrodes that showed higher variance activity relative to the rest of the population. Despite our best efforts, it is still possible that pathological activity may explain some of the observed relationships between complexity metrics and memory performance. In this scenario, however, the interpretation of our data does not change since decreased neural signal complexity, regardless of whether it can be attributed partly to epilepsy or to other factors, would still be related to decreased memory ability. Previous studies have indeed shown that interictal epileptiform discharges (IEDs) during encoding and retrieval can impair memory performance (Horak et al., 2017), and IED rates decrease from baseline during correct, but not incorrect, encoding trials (Matsumoto et al., 2013). Critically, however, increases in IEDs during rest or distractor periods in these studies do not appear to reduce memory performance, and the overall IED rates do not relate to recall performance across participants (Horak et al., 2017). This is in contrast to the effects we report here, which are observed during both rest and task periods. Moreover, controlling for the same level of overall pathology within individuals, we find the same metrics were related to memory performance across multiple timescales. It is difficult to explain how pathologic activity would consistently predict memory performance at every different timescale, or even why most effects in our data also extend to non-pathologic frontal lobe clusters. Hence, although the participants' underlying disorder may certainly affect normal neural information processing, our data suggest that the individual differences in neural signal complexity that relate to differences in memory performance are unlikely to be driven by pathology alone.

Finally, it is also possible that the changes in neural complexity that we interpret to denote cognitive flexibility in fact simply capture changing levels of attention. For example, patients may feel drowsier in some experimental sessions than others and these differences in levels of engagement may be captured by our complexity metrics. However, we note that changes in sample entropy from baseline to encoding states also occur over shorter timescales within an individual experimental session. These fine-grained temporal changes consistently capture differences between successful and unsuccessful associative memory encoding trials even though the baseline entropy levels are not different between the two conditions. Moreover, at the other extreme of time scales, participant-level complexity metrics correlate with memory performance as well as IQ. Therefore, it is unlikely that drowiness explains all of the observed relationships found here between neural complexity and memory performance at multiple scales. Attention may indeed play a direct role in determining the extent to which neural state space is explored during a task. However,

the possibility that changing levels of attention may explain our results is still consistent with the interpretation that theta power, spectral slope, and sample entropy ultimately reflect cognitive flexibility and a capacity to encode information.

Together, our data therefore provide insight into why memory performance may be variable both between and within individuals. Our data suggest that how well one can encode and retrieve memories is related to the flexibility in their cognitive processing. Such flexibility is captured directly by measuring the sample entropy of the neural signal, and corroborated by our measures of low frequency power and the PSD slope. People with better memory have neural signals that exhibit greater complexity, and therefore are capable of exhibiting more flexible behavior that is beneficial for memory formation.

References

Averbeck, B. B., Latham, P. E., and Pouget, A. (2006). Neural correlations, population coding and computation. *Nature Reviews. Neuroscience*, 7(5):358–366.

Binder, J. R., Desai, R. H., Graves, W. W., and Conant, L. L. (2009). Where is the semantic system? a critical review and meta-analysis of 120 functional neuroimaging studies. *Cerebral Cortex*, 19(12):2767–2796.

Bosl, W., Tierney, A., Tager-Flusberg, H., and Nelson, C. (2011). EEG complexity as a biomarker for autism spectrum disorder risk. *BMC Medicine*, 9:18.

Burke, J. F., Long, N. M., Zaghloul, K. A., Sharan, A. D., Sperling, M. R., and Kahana, M. J. (2014). Human intracranial high-frequency activity maps episodic memory formation in space and time. *NeuroImage*, 85:834–843.

Burke, J. F., Ramayya, A. G., and Kahana, M. J. (2015). Human intracranial high-frequency activity during memory processing: neural oscillations or stochastic volatility? *Current Opinion in Neurobiology*, 31:104–110.

Catarino, A., Churches, O., Baron-Cohen, S., Andrade, A., and Ring, H. (2011). Atypical eeg complexity in autism spectrum conditions: a multiscale entropy analysis. *Clinical Neurophysiology*, 122(12):2375–2383.

Churchill, N. W., Spring, R., Grady, C., Cimprich, B., Askren, M. K., Reuter-Lorenz, P. A., Jung, M. S., Peltier, S., Strother, S. C., and Berman, M. G. (2016). The suppression of scale-free fMRI brain dynamics across three different sources of effort: aging, task novelty and task difficulty. *Scientific Reports*, 6:srep30895.

Deco, G., Jirsa, V., McIntosh, A. R., Sporns, O., and Kötter, R. (2009). Key role of coupling, delay, and noise in resting brain fluctuations. *Proceedings of the National Academy of Sciences of the United States of America*, 106(25):10302–10307.

Deco, G. and Jirsa, V. K. (2012). Ongoing cortical activity at rest: criticality, multistability, and ghost attractors. *The Journal of Neuroscience: The Official Journal of the Society for Neuroscience*, 32(10):3366–3375.

Deco, G., Jirsa, V. K., and McIntosh, A. R. (2013). Resting brains never rest: computational insights into potential cognitive architectures. *Trends in Neurosciences*, 36(5):268–274.

Dehghani, N., Bédard, C., Cash, S. S., Halgren, E., and Destexhe, A. (2010). Comparative power spectral analysis of simultaneous elecroencephalographic and magnetoencephalographic recordings in humans suggests non-resistive extracellular media. *Journal of Computational Neuroscience*, 29(3):405–421.

Faisal, A. A., Selen, L. P. J., and Wolpert, D. M. (2008). Noise in the nervous system. *Nature Reviews in the Neurosciences*, 9:292 – 303.

Fell, J., Ludowig, E., Staresina, B., Wagner, T., Kranz, T., Elger, C. E., and Axmacher, N. (2011). Medial temporal theta/alpha power enhancement precedes successful memory encoding: evidence based on intracranial eeg. *The Journal of Neuroscience*, 31(14):5392–5397.

Freeman, W. J. and Zhai, J. (2009). Simulated power spectral density (PSD) of background electrocorticogram (ECoG). *Cognitive Neurodynamics*, 3(1):97–103.

Gao, R., Peterson, E. J., and Voytek, B. (2017). Inferring synaptic excitation/inhibition balance from field potentials. *NeuroImage*, 158:70–78.

Garrett, D. D., Kovacevic, N., McIntosh, A. R., and Grady, C. L. (2011). The importance of being variable. *The Journal of neuroscience : the official journal of the Society for Neuroscience*, 31(12):4496–4503.

Garrett, D. D., Samanez-Larkin, G. R., MacDonald, S. W., Lindenberger, U., McIntosh, A. R., and Grady, C. L. (2013). Moment-to-moment brain signal variability: A next frontier in human brain mapping? *Neuroscience and biobehavioral reviews*, 37(4):610–624.

Ghosh, A., Rho, Y., McIntosh, A. R., Kötter, R., and Jirsa, V. K. (2008). Noise during Rest Enables the Exploration of the Brain's Dynamic Repertoire. *PLoS Computational Biology*, 4(10).

Grady, C. L. and Garrett, D. D. (2014). Understanding Variability in the BOLD Signal and Why it Matters for Aging. *Brain imaging and behavior*, 8(2):274–283.

Greenberg, J. A., Burke, J. F., Haque, R., Kahana, M. J., and Zaghloul, K. A. (2015). Decreases in theta and increases in high frequency activity underlie associative memory encoding. *Neuroimage*, 114:257–263.

Guderian, S., Schott, B., Richardson-Klavehn, A., and Duzel, E. (2009). Medial temporal theta state before an event predicts episodic encoding success in humans. *Proceedings of the National Academy of Sciences*, 106(13):5365.

Hanslmayr, S., Aslan, A., Staudigl, T., Klimesch, W., Herrmann, C. S., and Bäuml, K.-H. (2007). Prestimulus oscillations predict visual perception performance between and within subjects. *NeuroImage*, 37(4):1465–1473.

Hanslmayr, S., Staresina, B., and Bowman, H. (2016). Oscillations and episodic memory: Addressing the synchronization/desynchronization conundrum. *Trends in Neurosciences*, 39(1).

Hanslmayr, S. and Staudigl, T. (2014). How brain oscillations form memories — A processing based perspective on oscillatory subsequent memory effects. *NeuroImage*, 85, Part 2:648–655.

Hanslmayr, S., Staudigl, T., and Fellner, M. (2012). Oscillatory power decreases and long-term memory: the information via desynchronization hypothesis. *Frontiers in Human Neuroscience*, 6.

Hanslmayr, S., Volberg, G., Wimber, M., Raabe, M., Greenlee, M. W., and Bäumel, K. H. T. (2011). The relationship between brain oscillations and bold signal during memory formation: A combined eeg-fmri study. *The journal of Neuroscience*, 31(44):15674–15680.

Haque, R., Wittig Jr., J., Damera, S., Inati, S. K., and Zaghloul, K. A. (2015). Cortical low-frequency power and progressive phase synchrony precede successful memory encoding. *Journal of Neuroscience*.

He, B., Zempel, J., Snyder, A., and Raichle, M. (2010). The temporal structures and functional significance of scale-free brain activity. *Neuron*, 66(3):353–369.

He, B. J. (2011). Scale-Free Properties of the Functional Magnetic Resonance Imaging Signal during Rest and Task. *Journal of Neuroscience*, 31(39):13786–13795.

He, B. J. (2014). Scale-free brain activity: past, present, and future. *Trends in Cognitive Sciences*, 18(9):480–487.

Heisz, J. J., Shedden, J. M., and McIntosh, A. R. (2012). Relating brain signal variability to knowledge representation. *NeuroImage*, 63(3):1384–1392.

Horak, P. C., Meisenhelter, S., Song, Y., Testorf, M. E., Kahana, M. J., Viles, W. D., Bujarski, K. A., Connolly, A. C., Robbins, A. A., Sperling, M. R., Sharan, A. D., Worrell, G. A., Miller, L. R., Gross, R. E., Davis, K. A., Roberts, D. W., Lega, B., Sheth, S. A., Zaghloul, K. A., Stein, J. M., Das, S. R., Rizzuto, D. S., and Jobst, B. C. (2017). Interictal epileptiform discharges impair word recall in multiple brain areas. *Epilepsia*, 58(3):373–380.

Jang, A. I., Wittig, J. H., Inati, S. K., and Zaghloul, K. A. (2017). Human Cortical Neurons in the Anterior Temporal Lobe Reinstate Spiking Activity during Verbal Memory Retrieval. *Current Biology*, 27(11):1700–1705.e5.

Kahana, M. J., Howard, M. W., and Polyn, S. M. (2008). Associative retrieval processes in episodic memory. In Roediger, III, H. L., editor, *Cognitive psychology of memory. Vol. 2 of Learning and memory: A comprehensive reference, 4 vols. (J. Byrne, Editor)*. Elsevier, Oxford.

Keshner, M. S. (1982). 1/f noise. *Proceedings of the IEEE*, 70(3):212–218.

Long, N. M., Burke, J. F., and Kahana, M. J. (2014). Subsequent memory effect in intracranial and scalp eeg. *NeuroImage*, 84:488–494.

MacDonald, S. W. S., Nyberg, L., and Bäckman, L. (2006). Intra-individual variability in behavior: links to brain structure, neurotransmission and neuronal activity. *Trends in Neurosciences*, 29(8):474–480.

Madan, C., Glaholt, M., and Caplan, J. (2010). The influence of item properties on association-memory. *Journal of Memory and Language*, 63:46–63.

Manning, J. R., Jacobs, J., Fried, I., and Kahana, M. J. (2009). Broadband shifts in LFP power spectra are correlated with single-neuron spiking in humans. *J Neurosci*, 29(43):13613 – 13620.

Maris, E. and Oostenveld, R. (2007). Nonparametric statistical testing of EEG- and MEG-data. *J. Neurosci. Methods*, 164:177–190.

Matsumoto, J. Y., Stead, M., Kucewicz, M. T., Matsumoto, A. J., Peters, P. A., Brinkmann, B. H., Danstrom, J. C., Goerss, S. J., Marsh, W. R., Meyer, F. B., et al. (2013). Network oscillations modulate interictal epileptiform spike rate during human memory. *Brain*.

McIntosh, A. R., Kovacevic, N., and Itier, R. J. (2008). Increased Brain Signal Variability Accompanies Lower Behavioral Variability in Development. *PLOS Computational Biology*, 4(7):e1000106.

Miller, K. J., Sorensen, L. B., Ojemann, J. G., den Nijs, M., and Sporns, O. (2009). Power-law scaling in the brain surface electric potential. *PLoS Comput Biol*, 5(12):e1000609.

Milstein, J., Mormann, F., Fried, I., and Koch, C. (2009). Neuronal shot noise and Brownian $1/f^2$ behavior in the local field potential. *PLoS One*, 4(2):e4338.

Misić, B., Mills, T., Taylor, M. J., and McIntosh, A. R. (2010). Brain noise is task dependent and region specific. *Journal of Neurophysiology*, 104(5):2667–2676.

Mišić, B., Vakorin, V. A., Paus, T., and McIntosh, A. R. (2011). Functional Embedding Predicts the Variability of Neural Activity. *Frontiers in Systems Neuroscience*, 5.

Mitchell, J. F., Sundberg, K. A., and Reynolds, J. H. (2009). Spatial attention decorrelates intrinsic activity fluctuations in macaque area v4. *Neuron*, 63(6):879–888.

Mizuno, T., Takahashi, T., Cho, R., Kikuchi, M., Murata, T., Takahashi, K., and Wada, Y. (2010). Assessment of eeg dynamical complexity in alzheimer's disease using multiscale entropy. *Clinical Neurophysiology*, 121(9):1438–1446.

Nimon, K., Lewis, M., Kane, R., and Haynes, R. M. (2008). An R package to compute commonality coefficients in the multiple regression case: an introduction to the package and a practical example. *Behavior Research Methods*, 40(2):457–466.

Nimon, K., Oswald, F., and Roberts., J. K. (2013). *yhat: Interpreting Regression Effects*, r package version 2.0-0 edition.

Nunez, P. L. and Srinivasan, R. (2006). *Electric Fields of the Brain*. Oxford University Press, New York.

Osipova, D., Takashima, A., Oostenveld, R., Fernndez, G., Maris, E., and Jensen, O. (2006). Theta and gamma oscillations predict encoding and retrieval of declarative memory. *J Neurosci*, 26(28):7523–7531.

Podvalny, E., Noy, N., Harel, M., Bickel, S., Chechik, G., Schroeder, C. E., Mehta, A. D., Tsodyks, M., and Malach, R. (2015). A unifying principle underlying the extracellular field potential spectral responses in the human cortex. *Journal of Neurophysiology*, 114(1):505–519.

Pozzorini, C., Naud, R., Mensi, S., and Gerstner, W. (2013). Temporal whitening by power-law adaptation in neocortical neurons. *Nature Neuroscience*, 16(7):942–948.

Protzner, A. B., Valiante, T. A., Kovacevic, N., McCormick, C., and McAndrews, M. P. (2010). Hippocampal signal complexity in mesial temporal lobe epilepsy: a noisy brain is a healthy brain. *Archives Italiennes De Biologie*, 148(3):289–297.

709 Ralph, M. A. L., Jefferies, E., Patterson, K., and Rogers, T. T. (2017). The neural and computational bases of
710 semantic cognition. *Nature Reviews Neuroscience*, 18(1):42–55.

711 Ray, S. and Maunsell, J. H. R. (2011). Different origins of gamma rhythm and high-gamma activity in macaque
712 visual cortex. *PLOS Biology*, 9(4):1–15.

713 Richman, J. S. and Moorman, J. R. (2000). Physiological time-series analysis using approximate entropy and sample
714 entropy. *American Journal of Physiology. Heart and Circulatory Physiology*, 278(6):H2039–2049.

715 Schneidman, E., Puchalla, J. L., Segev, R., Harris, R. A., Bialek, W., and Berry, M. J. (2011). Synergy from silence
716 in a combinatorial neural code. *J Neurosci*, 31(44):15732–15741.

717 Sederberg, P. B., Gauthier, L. V., Terushkin, V., Miller, J. F., Barnathan, J. A., and Kahana, M. J. (2006). Oscillatory
718 correlates of the primacy effect in episodic memory. *NeuroImage*, 32(3):1422–1431.

719 Sederberg, P. B., Kahana, M. J., Howard, M. W., Donner, E. J., and Madsen, J. R. (2003). Theta and gamma
720 oscillations during encoding predict subsequent recall. *Journal of Neuroscience*, 23(34):10809–10814.

721 Sederberg, P. B., Schulze-Bonhage, A., Madsen, J. R., Bromfield, E. B., McCarthy, D. C., Brandt, A., Tully, M. S.,
722 and Kahana, M. J. (2007). Hippocampal and neocortical gamma oscillations predict memory formation in humans.
723 *Cerebral Cortex*, 17(5):1190–1196.

724 Shew, W. L., Yang, H., Petermann, T., Roy, R., and Plenz, D. (2009). Neuronal Avalanches Imply Maximum
725 Dynamic Range in Cortical Networks at Criticality. *The Journal of Neuroscience*, 29(49):15595–15600.

726 Shew, W. L., Yang, H., Yu, S., Roy, R., and Plenz, D. (2011). Information Capacity and Transmission Are Maximized
727 in Balanced Cortical Networks with Neuronal Avalanches. *The Journal of neuroscience : the official journal of*
728 *the Society for Neuroscience*, 31(1):55–63.

729 Sleimen-Malkoun, R., Perdikis, D., Müller, V., Blanc, J.-L., Huys, R., Temprado, J.-J., and Jirsa, V. K. (2015).
730 Brain Dynamics of Aging: Multiscale Variability of EEG Signals at Rest and during an Auditory Oddball Task". .
731 *eNeuro*, 2(3):ENEURO.0067–14.2015.

732 Sokunbi, M. O. (2014). Sample entropy reveals high discriminative power between young and elderly adults in short
733 fMRI data sets. *Frontiers in Neuroinformatics*, 8.

734 Sokunbi, M. O., Fung, W., Sawlani, V., Choppin, S., Linden, D. E. J., and Thome, J. (2013). Resting state
735 fMRI entropy probes complexity of brain activity in adults with ADHD. *Psychiatry Research: Neuroimaging*,
736 214(3):341–348.

737 Stein, R. B., Gossen, E. R., and Jones, K. E. (2005). Neuronal variability: noise or part of the signal? *Nature*
738 *Reviews. Neuroscience*, 6(5):389–397.

Usher, M., Stemmler, M., and Olami, Z. (1995). Dynamic Pattern Formation Leads to $\frac{1}{f}$ Noise in Neural Populations. *Physical Review Letters*, 74(2):326–329.

Vakorin, V. and McIntosh, A. R. (2012). Mapping the Multiscale Information Content of Complex Brain Signals. In *Principles of Brain Dynamics: Global State Interactions, 2012, ISBN 978-0-262-01764-0, págs. 184-208*, pages 184–208.

Vaz, A. P., Yaffe, R. B., Jr, J. H. W., Inati, S. K., and Zaghloul, K. A. (2017). Dual origins of measured phase-amplitude coupling reveal distinct neural mechanisms underlying episodic memory in the human cortex. *NeuroImage*, 148:148 – 159.

Voytek, B., Kayser, A., Badre, D., Fegen, D., Chang, E., Crone, N., Parvizi, J., Knight, R., and D'Esposito, M. (2015). Oscillatory dynamics in human frontal networks in support of goal maintenance. *Nat Neurosci*, 18(9):1318–1324.

Voytek, B. and Knight, R. T. (2015). Dynamic network communication as a unifying neural basis for cognition, development, aging, and disease. *Biological Psychiatry*, 77(12):1089–1097.

Yaffe, R. B., Kerr, M. S. D., Damera, S., Sarma, S. V., Inati, S. K., and Zaghloul, K. A. (2014). Reinstatement of distributed cortical oscillations occurs with precise spatiotemporal dynamics during successful memory retrieval. *Proceedings of the National Academy of Sciences*, 111(52):18727–18732.

Yaffe, R. B., Shaikhouni, A., Arai, J., Inati, S. K., and Zaghloul, K. A. (2017). Cued Memory Retrieval Exhibits Reinstatement of High Gamma Power on a Faster Timescale in the Left Temporal Lobe and Prefrontal Cortex. *Journal of Neuroscience*, pages 3810–16.

Yentes, J. M., Hunt, N., Schmid, K. K., Kaipust, J. P., McGrath, D., and Stergiou, N. (2013). The appropriate use of approximate entropy and sample entropy with short data sets. *Annals of Biomedical Engineering*, 41(2):349–365.

Tables

Table 1 Commonality analysis output describing unique and common contributions of the three predictor variables (theta-band power, spectral slope, and sample entropy) to the regression effect explaining memory performance across participants.

	power	**spectral slope**	**sample entropy**	**% Total**
Unique to power	0.1461			37.60
Unique to spectral slope		0.0414		10.66
Unique to sample entropy			0.0049	1.25
Common to power and spectral slope	0.0390	0.0390		10.03
Common to power and sample entropy	0.0232		0.0232	5.97
Common to spectral slope and sample entropy		0.0341	0.0341	8.77
Common to power, spectral slope, and sample entropy	0.0999	0.0999	0.0999	25.72

Total $R^2 = 0.3885$. Unique + Common = 100% of R^2.

Figure Legends

Figure 1 Paired associates task and subject distribution (A) Paired associates memory task schematic. (B) Average performance distribution across subjects, distribution is bimodal ranging between 0.05 and 0.84 with a median accuracy of 0.36 (N=43). (C) Electrode coverage by spatial region of interest. Colormap reflects number of electrodes within 12.5 mm. (D) Correlation between full-scale IQ and accuracy across subjects $r_s = 0.55,\ p = .0005,\ N = 36$. Line is standard least squares regression line.

Figure 2 Baseline Power and Performance. (A) Average log_{10} broadband power across all trials and electrodes, range 5.21 to 7.46 (arbitrary units) is negatively correlated with performance r_s = -.38, $p = .012,\ N = 43$. Line is standard least squares regression line. (B) Power ˜accuracy correlation by frequency band. The negative correlation between power and accuracy exists across all bands and is significantly negatively correlated at all frequency bands below 10 Hz ($p < .05$, Bonferroni correct for 30 frequency bands). The error bars indicate standard error of the mean for Spearman's correlation ($\frac{0.6325}{\sqrt{n-1}}$). Theta power spectral region of interest is inside of dashed box. (C) Broadband (fisher transformed) correlation across spatial ROIs. Lower panel shows regions significant ($p < .05$) compared to a permuted distribution through a clustering procedure. (D) Same as C for theta band power.

Figure 3 Spectral Slope and Performance. (A) Average power spectral density across tertials of subjects sorted by performance, shading shows standard error of the mean. (B) Distribution of average spectral slopes across subjects $2.71 \pm .05$ ($mean \pm SEM$). Insert shows example subject, red is range of frequencies slope is calculated over (10-100 Hz) and dashed line shows robust fit line. (C) Spectral slope is positively correlated with accuracy across subjects $r_s = 0.49,\ p = .0011,\ N = 43$. Line is standard least squares regression line. (D) Correlation of spectral slope and accuracy across spatial ROIs. Lower panel shows regions significant ($p < .05$) compared to a permuted distribution through a clustering procedure. (E) Average spectral slope as a function of center frequency and spectral width. White star indicates parameters for previous slope values.(F) Average correlation as a function of center frequency and spectral width as in (E).

Figure 4 Sample Entropy and Performance. (A) Sample entropy schematic for theoretical signals. Color of dots superimposed on signals indicate discretized voltage bin. Signal y_2 is more complex than y_1 making subsequent points relatively more difficult to predict. (B) Example epochs from two participants with low and high entropy. The upper signal is from participant with an average sampEn of 0.51, this epoch has a measured sampEn of 0.67. The lower signal is from participant with an average sample Entropy of 1.29, this epoch has a measured sample Entropy of 1.51. (C) Sample entropy is positively correlated with performance across participants $r_s = 0.51,\ p = .0005$. Line is standard least squares regression line. (D) Sample entropy correlation across spatial ROIs. Lower panel shows

794 regions significant ($p < .05$) compared to a permuted distribution through a clustering procedure.

795

796 **Figure 5** Sample Entropy across Time Scales. (A) Example subject with positive session level correlation of sample
797 entropy to accuracy (B) Distribution of fisher transformed ρ values across subjects is significantly greater than 0
798 ($t(22) = 3.35,\ p = .003$)(C) Population average session correlation by ROI (t-score). Lower panel shows regions
799 significant ($p < .05$) compared to a permuted distribution through a clustering procedure. (D) Example subject
800 level distribution of sample entropy values for correct vs. incorrect trials (E) Distribution of correct - incorrect
801 sample entropy across subjects is significantly greater than 0 ($t(43) = 2.89,\ p = .006$) (F) Population average change
802 in sample entropy by item (t-score) across ROIs. Lower panel shows regions significant ($p < .05$) compared to a
803 permuted distribution through a clustering procedure.

804

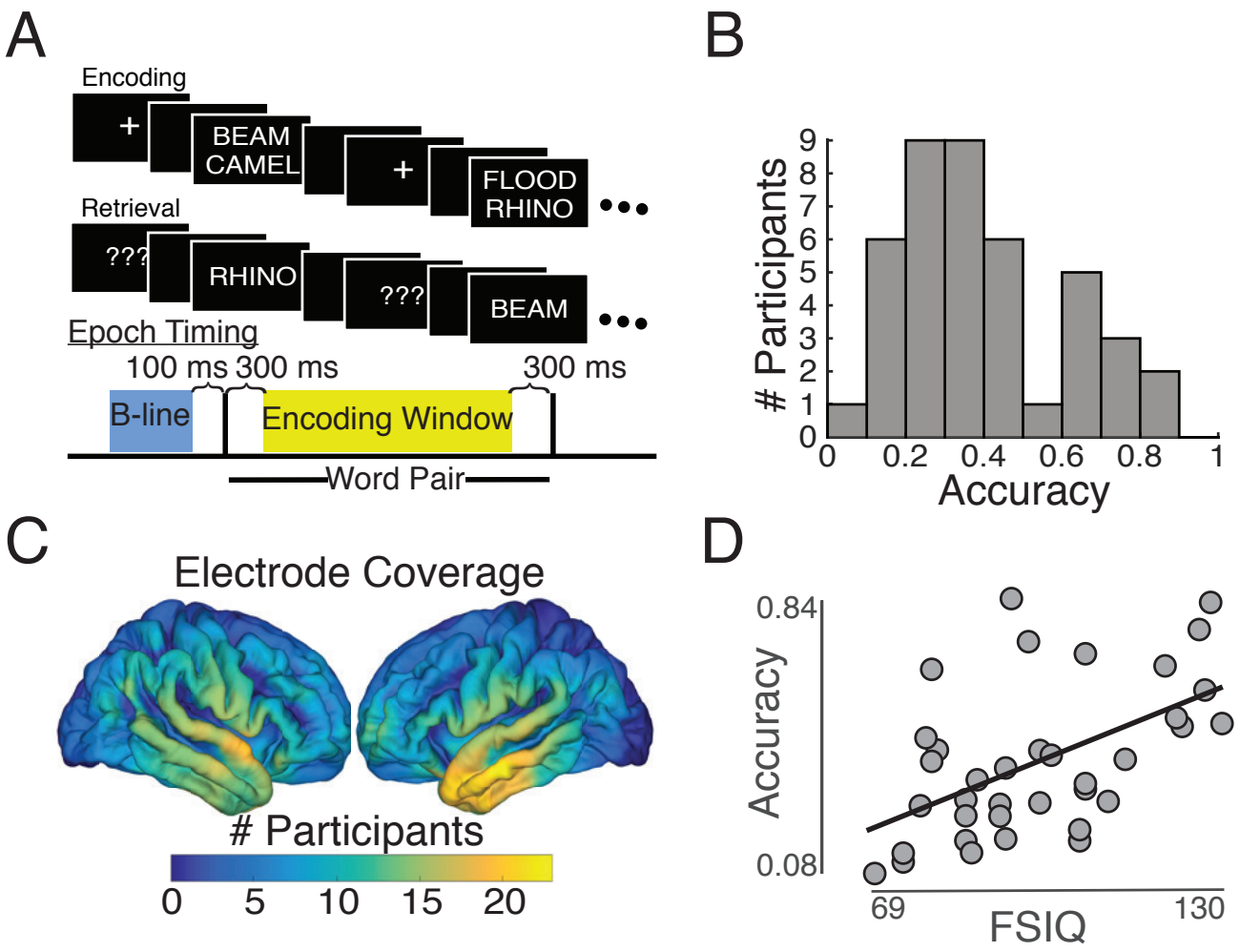

Figure 1

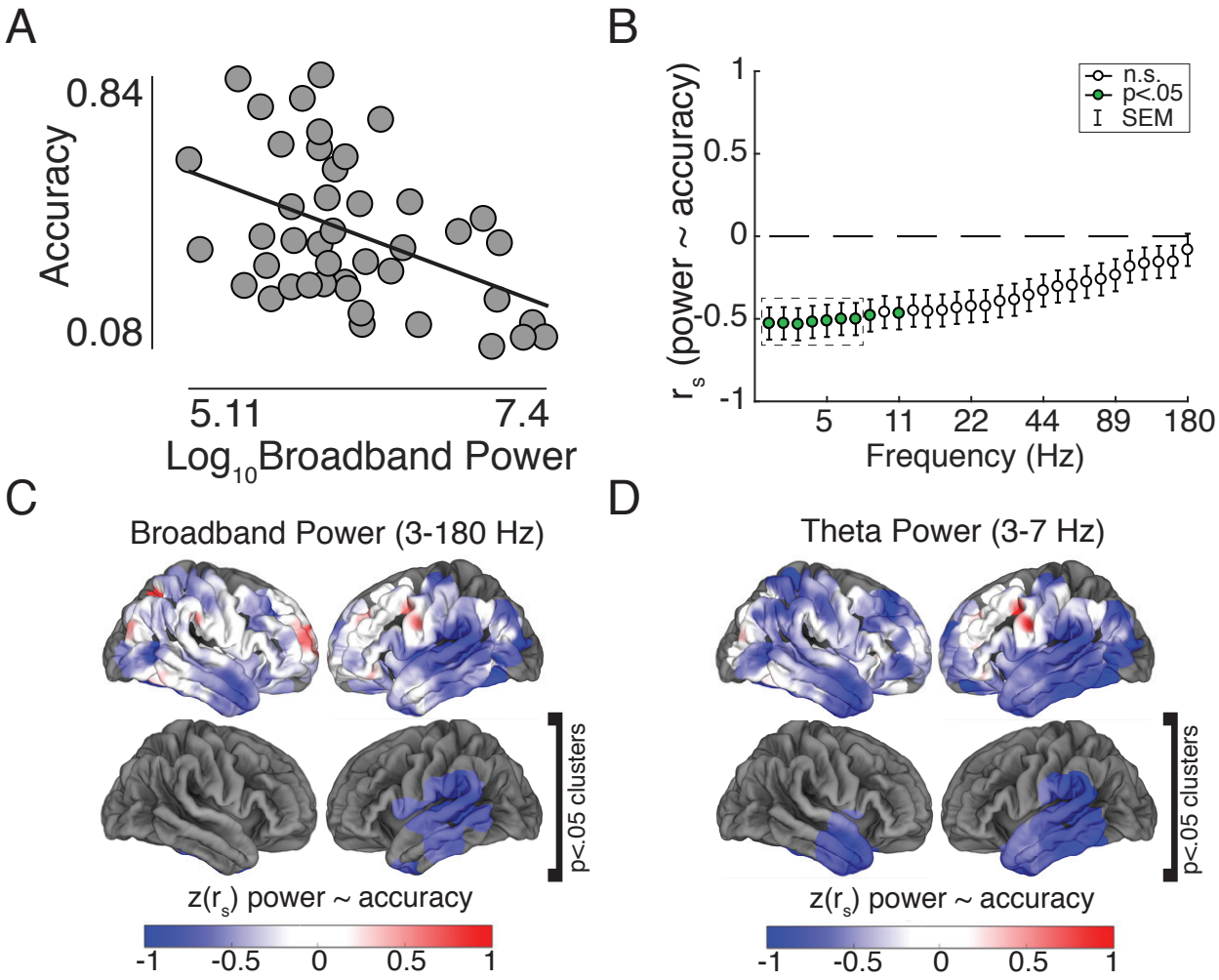

Figure 2

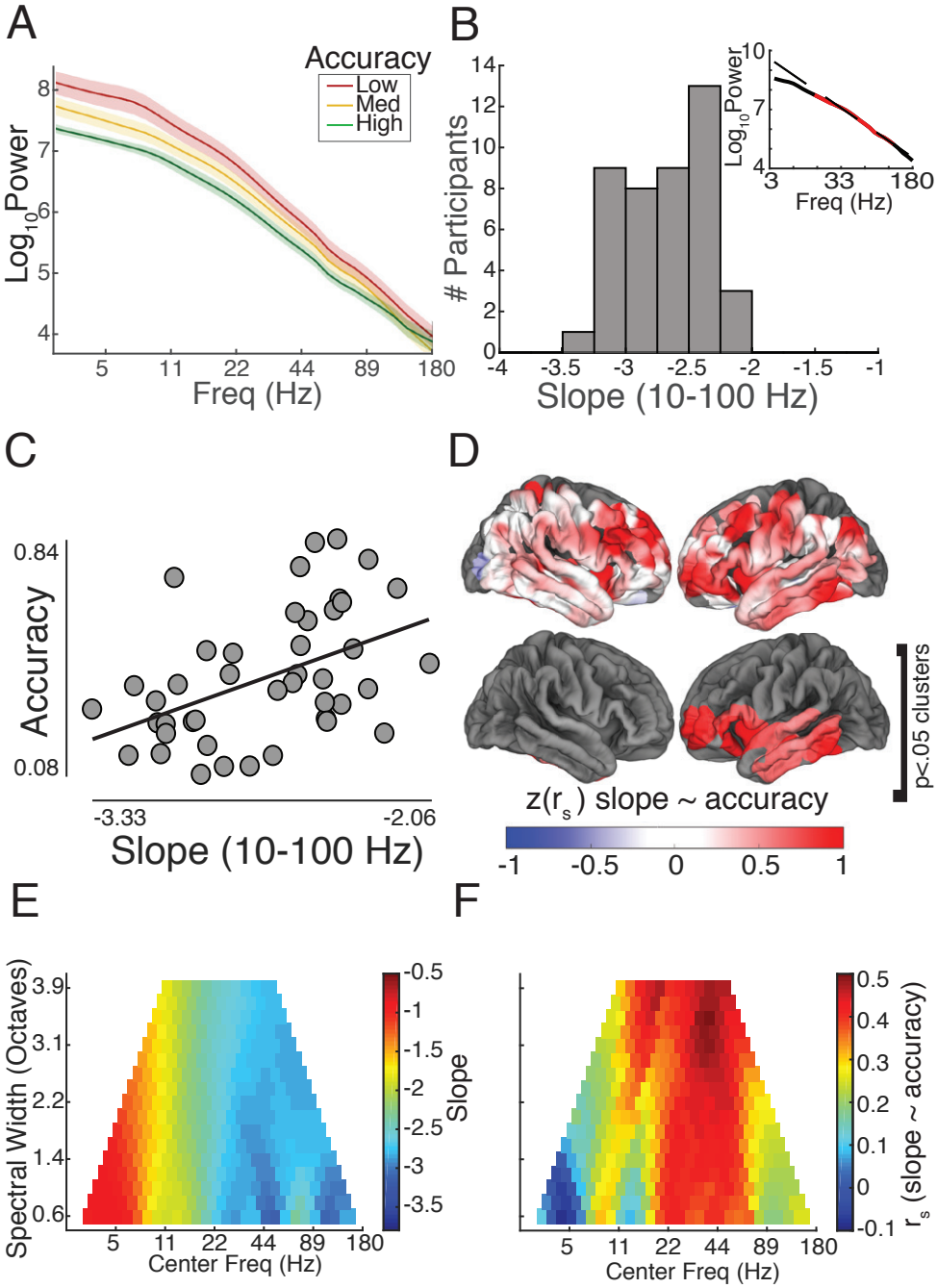

Figure 3

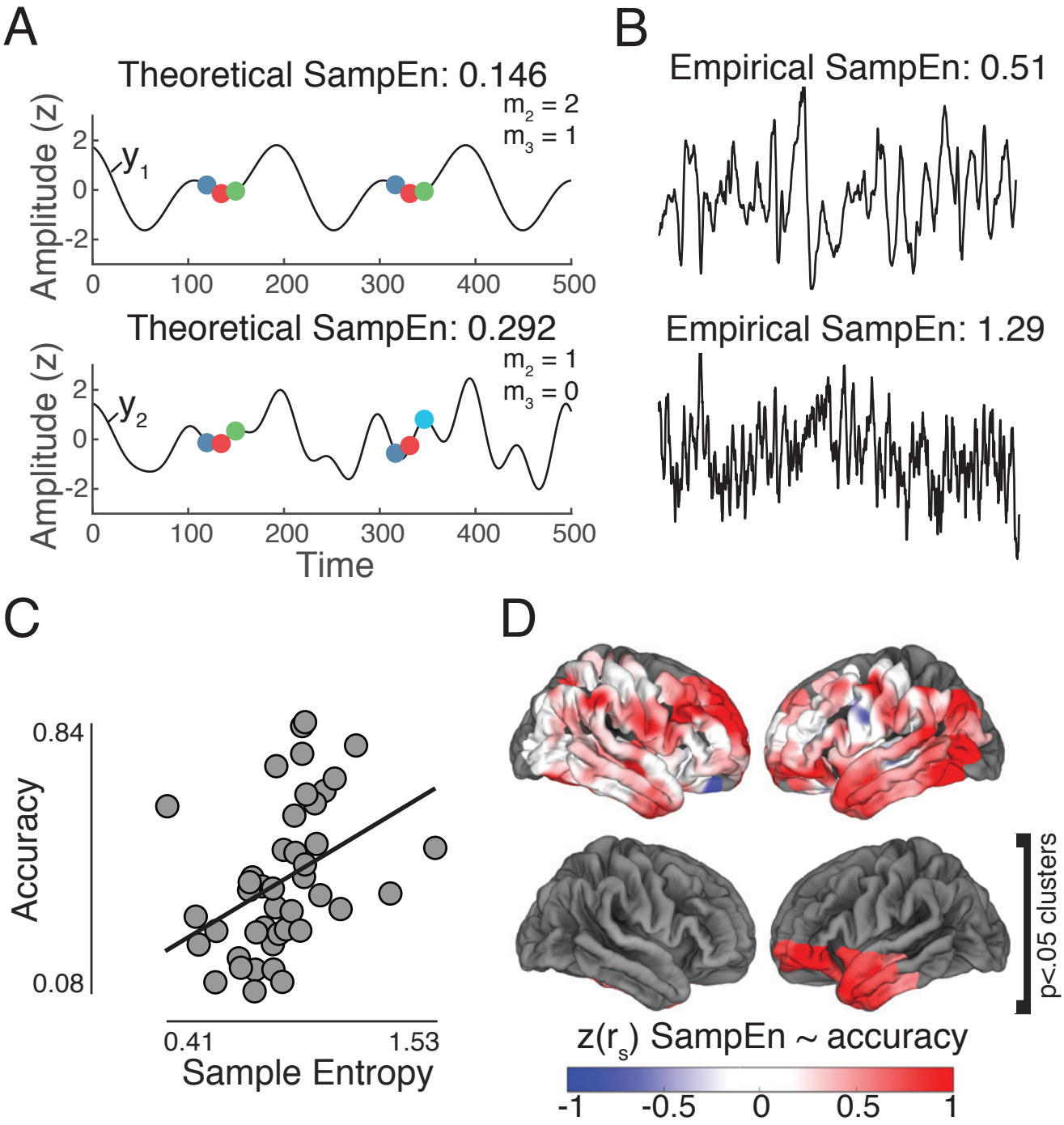

Figure 4

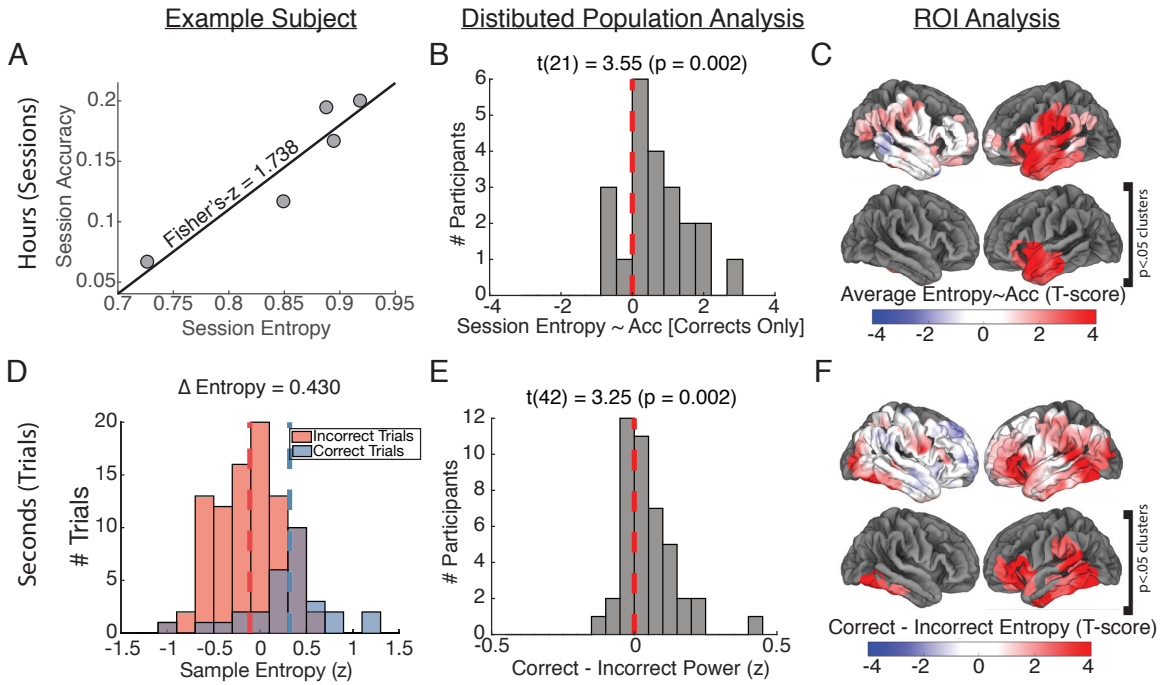

Figure 5